THE ASTRONOMICAL JOURNAL, 115:1319–1328, 1998 April

HIGH-z Lyα EMITTERS. I. A BLANK-FIELD SEARCH FOR OBJECTS NEAR REDSHIFT $z = 3.4$ IN AND AROUND THE HUBBLE DEEP FIELD AND THE HAWAII DEEP FIELD SSA 22[1]

LENNOX L. COWIE[2,3] AND ESTHER M. HU[2]
Institute for Astronomy, University of Hawaii, 2680 Woodlawn Drive, Honolulu, HI 96822; cowie@ifa.hawaii.edu, hu@ifa.hawaii.edu
Received 1997 November 18; revised 1998 January 6

ABSTRACT

We present deep narrowband ($\lambda = 5390$ Å, $\Delta\lambda = 77$ Å) and multicolor observations of the Hubble Deep Field and the Hawaii Deep Field SSA 22 obtained with the LRIS instrument at the 10 m Keck II Telescope. It is shown that there is a substantial population of galaxies at $z \sim 3.4$ that can be selected by Lyα emission. Comparison with color-selected samples shows that the samples selected with these different criteria have substantial, but not complete, overlap and that there is a comparable surface density in the two selected populations. The emission-line–selected samples include objects with strong Lyα, and which are significant contributers to the integrated star formation at these epochs. For a Salpeter initial mass function, we estimate a minimum star formation rate of 0.01 $M_\odot$ Mpc^{-3} yr^{-1} at $z = 3.4$ for $H_0 =$ 65 km s^{-1} Mpc^{-1} and $q_0 = 0.5$ in the Lyα-selected objects, though the value could be substantially higher if there is significant extinction.

Key words: cosmology: observations — early universe — galaxies: evolution — galaxies: formation

1. INTRODUCTION

Recent opinion has swung heavily to the viewpoint that emission-line searches for high-z Lyα emitters have failed, and that color-based searches may represent the only realistic way to identify high-redshift galaxies. In the present series of papers, we shall show that this assumption is ill-founded and that slightly more sensitive searches than previously carried out yield very large numbers of high-z Lyα emitters, including some objects that are so faint in the continuum that they would not be easily detected on the basis of their colors. The results show that emission-line searches using 10 m–class telescopes and either narrowband or spectroscopic techniques are an efficient means of identifying and studying the distribution and clustering of high-redshift galaxies, including objects beyond redshift 5.

Indeed, the pessimism has not been justified even based on existing data. Surveys around known objects have yielded numbers of Lyα emitters both at moderate z (Djorgovski et al. 1985; Macchetto et al. 1993; Francis et al. 1996; Pascarelle et al. 1996; Djorgovski et al. 1996; Francis, Woodgate, & Danks 1997) and high z (Hu, McMahon, & Egami 1996; Petitjean et al. 1996; Hu & McMahon 1996; Hu, McMahon, & Egami 1997), and while these results may be dismissed as a consequence of the possibly anomalous environments around the target objects, it is also true that quite a large fraction of the color-selected $z = 2$–4 objects have Lyα in emission (see Steidel et al. 1996a, 1996b; Lowenthal et al. 1997; Steidel et al. 1998). Indeed, these latter results show at once that blank-field objects can be found with only a small increase in sensitivity over the existing Lyα surveys summarized by Pritchet (1994).

A substantial gain in depth is now possible with the advent of the 10 m telescopes, and in order to exploit this we have begun a narrowband filter search for high-z Lyα emitters using the LRIS instrument (Oke et al. 1995) in imaging mode on the 10 m Keck II Telescope with specially designed filters. In the present paper, we describe observations of a 25.3 arcmin^2 region surrounding the Hubble Deep Field (HDF; Williams et al. 1996) and a similar area around the Hawaii Deep Field SSA 22 (Cowie et al. 1994) in broadband B, V, and I colors, using a filter centered at 5390 Å that covers a 77 Å bandpass. This filter would detect Lyα at $z = 3.405$–3.470. Subsequent papers in this series will address deep slit spectroscopy of quasar and blank fields, and deep optical and infrared narrowband imaging studies at higher redshifts. At the time of the filter design, no objects were known to lie within the filter redshift range, but subsequently one such object was identified by Lowenthal et al. (1997) in the HDF field itself. The search is therefore a blank-field search, but among the objects identified as Lyα emitters in this redshift interval, the survey does indeed recover the $z = 3.430$ object found by Lowenthal et al. (identified as hd2_0698_1297 in their paper).

SSA 22 and the HDF are ideal test areas for a narrowband imaging search because of the large number of spectroscopic redshift identifications in and around these areas and the ultradeep multicolor photometric information available in the HDF proper. Thus a survey using these fields allows us to address issues such as (1) comparing methodologies and sensitivities of narrowband emission-line techniques and continuum color-break techniques for identifying high-redshift galaxies, (2) determining relative numbers of foreground emission-line objects and determining the best methods for distinguishing between the various types of emitters (e.g., Lyα, [O II], Hβ, [O III]), (3) estimating the relative surface density of high-redshift candidates as a function of flux found using each technique, and (4) establishing a baseline for comparison between blank-field and targeted searches around high-z objects (such as radio galaxies, damped Lyα absorbers, and quasars), and for evolution of galaxy properties at higher redshifts. In addition, we can establish specified criteria (e.g., desired magnitude

[1] Based in part on observations with the NASA/ESA *Hubble Space Telescope*, obtained at the Space Telescope Science Institute, which is operated by the Association of Universities for Research in Astronomy (AURA), Inc., under NASA contract NAS 5-26555.

[2] Visiting Astronomer, W. M. Keck Observatory, jointly operated by the California Institute of Technology, the University of California, and the National Aeronautics and Space Administration.

[3] Visiting Astronomer, Canada-France-Hawaii Telescope, operated by the National Research Council of Canada, the Centre National de la Recherche Scientifique of France, and the University of Hawaii.

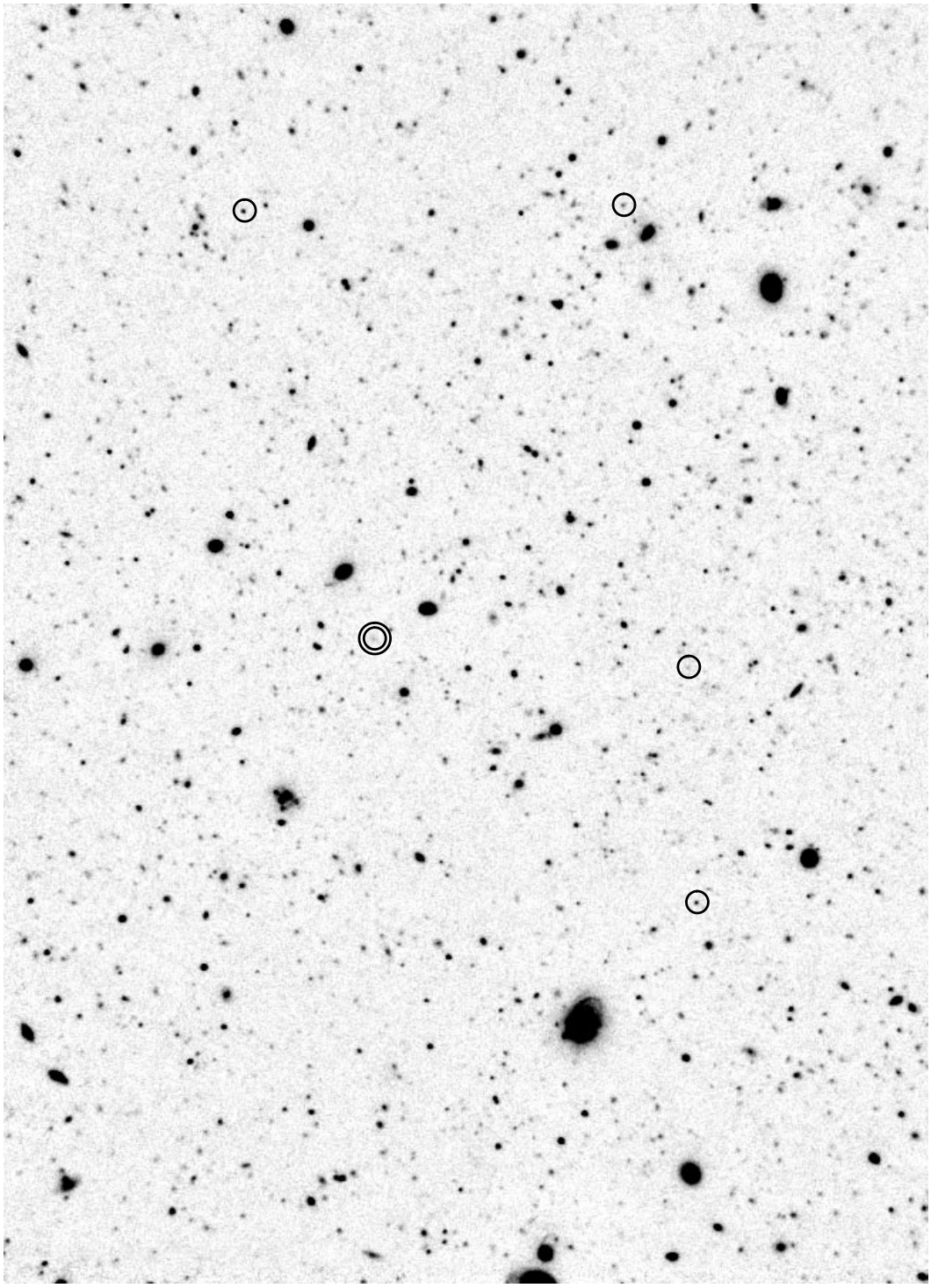

FIG. 1*a*

FIG. 1.—(*a*) Narrowband image of the HDF and surrounding field. The displayed field of view shows a 380″ × 275″ region from a 2 hr exposure taken with LRIS on the Keck II Telescope through a 5390 Å narrowband filter (77 Å FWHM) in the collimated beam. The composite image quality is ∼0.″7 FWHM, with a 1 σ limiting AB magnitude of 26.8 over a 3″ diameter aperture, corrected to a total magnitude following Cowie et al. (1994), and with a corresponding 1 σ flux of 6×10^{-18} ergs cm^{-2} s^{-1} over the same aperture. Circled items indicate field objects with narrowband equivalent widths in excess of 77 Å in the observed frame that also fall within the central 6.′0 × 4.′2 region used for the narrowband catalog (including objects brighter than the 5 σ limiting magnitude of 25). The twice-circled object is the one cataloged narrowband object that lies within the HDF proper (the LRIS field displayed covers an area 4.4 times larger than the HDF field). This has a redshift identification by Lowenthal et al. (1997) of $z = 3.430$ (their object hd2_0698_1297), in agreement with the Lyα selection of the filter. This is also the only object among currently reported galaxies lying within the HDF with a redshift that would place Lyα emission within the filter bandpass; however, we note that no information about object emission-line redshifts in the selected bandpass was available at the time the filter was designed. Circles correspond to a 4.″6 diameter aperture. Most of the indicated emission-line objects are more compact than the object identified by Lowenthal et al., as was generally true of the other high-redshift objects discussed in that paper. This object also lies at the lower end of our equivalent width selection criterion. (*b*) Narrowband image of the SSA 22 field. The field of view seen in this image is 390″ × 280″ and reaches a 1 σ flux of 3×10^{-18} ergs cm^{-2} s^{-1} over a 3″ diameter aperture for the 5 hr exposure. The circled objects correspond to objects whose emission is in excess of an equivalent width of 77 Å for $N(\mathrm{AB}) < 25.5$. North is to the left on the images.

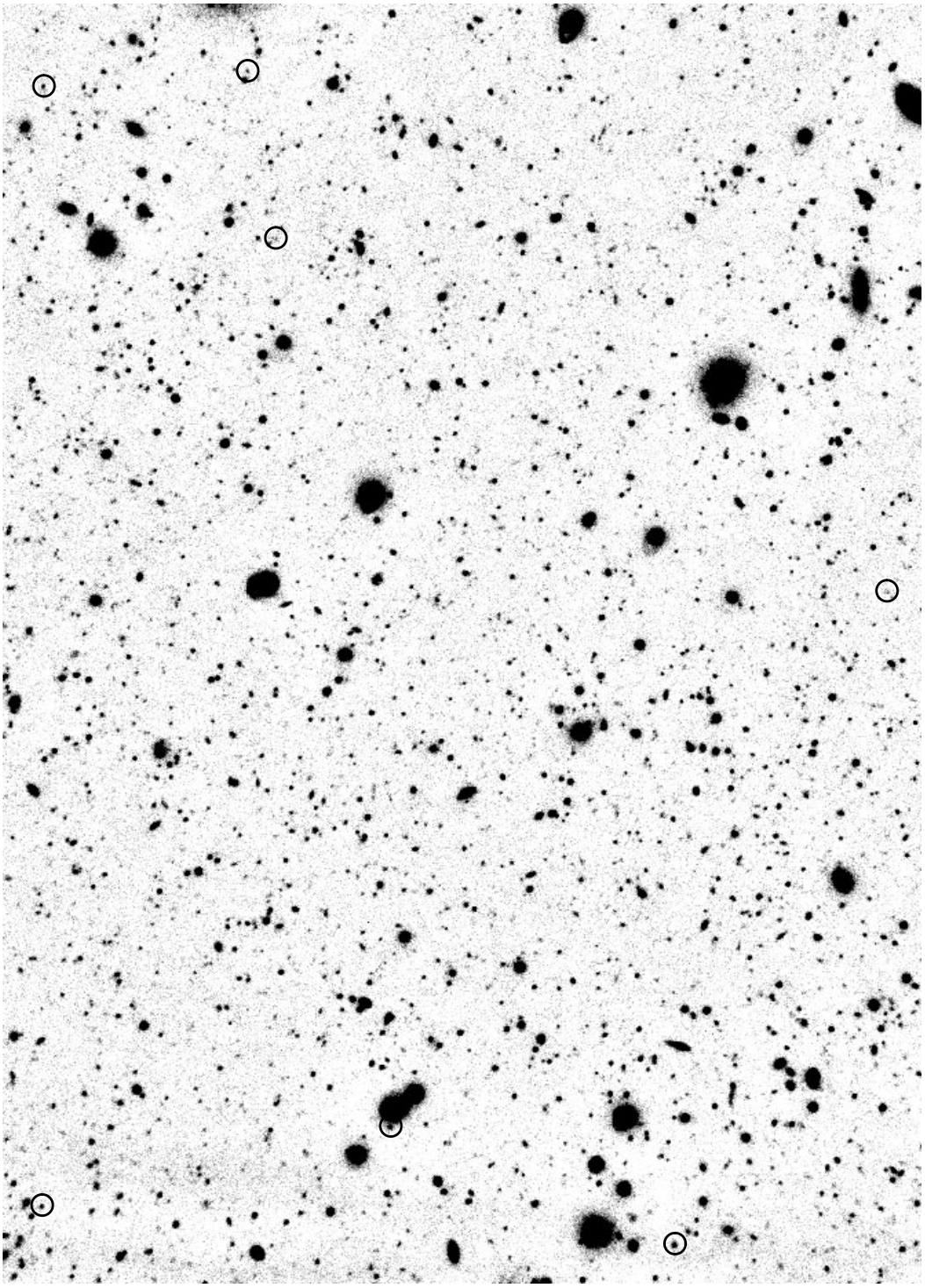

FIG. 1*b*

limits, required precision of color estimates for separating objects of different redshift, typical spatial extents) on well-studied fields with high-resolution images, which then permit fine-tuning future investigations of high-redshift galaxies. Finally, when used in conjunction with optical and infrared narrowband surveys currently in progress, the incidence and statistics of foreground emission-line objects are also of interest for estimating the surface densities of star-forming galaxies and active galactic nuclei (AGNs) at different epochs, and for comparing indexes such as [O II] with primary star formation indexes such as Hα (Kennicutt 1983, 1992) or the far-UV flux, in order to track the evolution of star formation history to very high redshifts. We shall address these issues in subsequent papers.

2. DATA

Narrowband observations using the LRIS camera were obtained on the Hubble Deep Field (HDF) on the night of UT 1997 May 2 and on SSA 22 on the nights of UT 1997 August 8 and 10. The narrowband filter was a specially

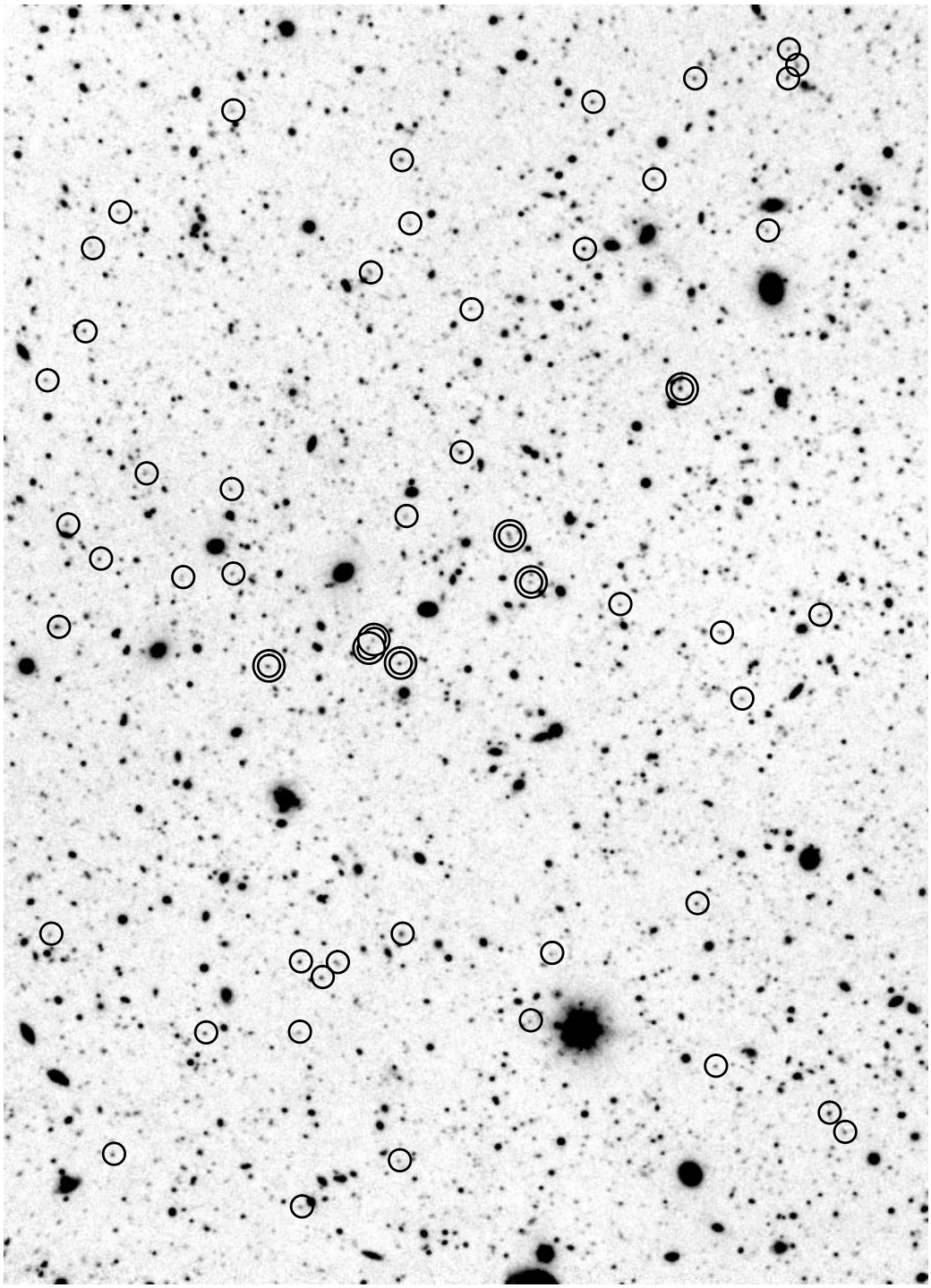

FIG. 2*a*

FIG. 2.—(*a*) V-band image of the HDF, comprising 0.6 hr on Keck II (LRIS) combined with 11 hr on CFHT with the UH8K mosaic CCD camera. The 1 σ (Johnson) V limit over a corrected 3″ diameter aperture is 27.4. Circled objects are selected from $V < 25.5$ objects that have red $B-V$ colors ($B-V \geq 1.1$) and blue $V-I$ colors ($V-I \leq 1.6$), many of which should correspond to high-redshift galaxies. Again, objects with double circles indicate galaxies that meet the selection criteria and also have measured redshifts, given in (*b*). Four of the remaining color-selected objects lie in the HDF proper. Of these, one (hd2_0853_0319) has a tentative redshift of $z = 3.35$ from Lowenthal et al. (1997). (*b*) Identifications of high-redshift galaxies in the HDF that have been spectroscopically identified by Lowenthal et al. (1997), in the Hawaii Active Catalog, or by Steidel et al. (1996a). (*c*) V-band image of SSA 22, with circled objects showing the color selection for high-redshift galaxies applied in (*a*), and with those galaxies with measured redshifts (known in the literature prior to our spectroscopic follow-up) indicated with double circles. The 1 σ V limit is 27.5. North is to the left on the images.

designed 9.″5 square interference filter centered at 5390 Å, with a peak transmission of just under 70% and FWHM of 77 Å, and located in the collimated beam at the standard LRIS filter position. The filter lies in a very dark region of sky and was also matched to a dark portion of the infrared sky where [O II] would lie if Lyα were in the optical narrow band. For the HDF, a series of 900 s exposures (2 hr) shifted by 15″ between successive frames were taken in the narrow-

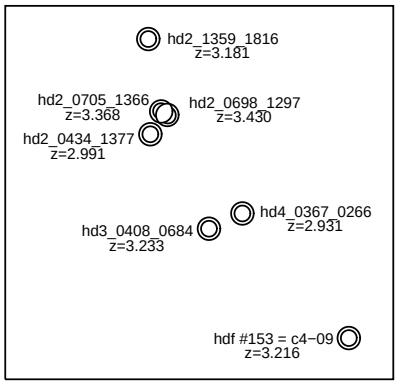
hd2_1359_1816
z=3.181
hd2_0705_1366
z=3.368
hd2_0698_1297
z=3.430
hd2_0434_1377
z=2.991
hd4_0367_0266
z=2.931
hd3_0408_0684
z=3.233
hdf #153 = c4−09
z=3.216

FIG. 2*b*

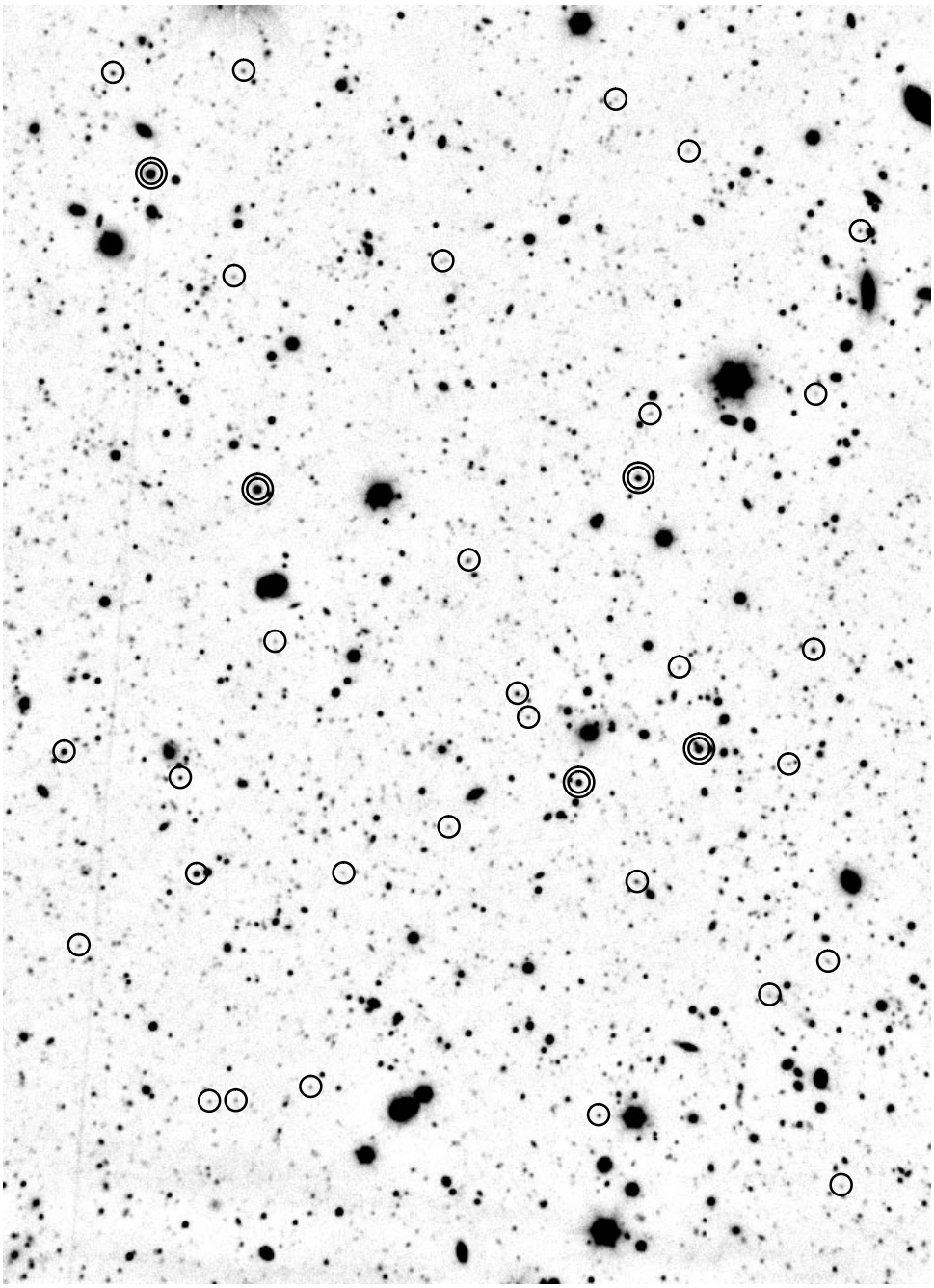

FIG. 2*c*

band filter, immediately followed by a series of 360 s V-band exposures (0.6 hr) on the same field. These data were combined with a series of 420 s B-band exposures (0.7 hr) taken with LRIS on the night of UT 1997 March 8. For SSA 22, a 5 hr narrowband exposure was taken, again as a series of 900 s exposures, while the B data were acquired as a series of 420 s exposures (0.8 hr) on UT 1997 August 9, with the V data taken as a series of 400 s exposures over the nights of UT 1997 August 8 and 10 (1.6 hr), and I data taken as a series of 300 s exposures on UT 1997 August 10 (0.7 hr). The data were processed using median sky flats generated from the dithered images and calibrated using observations of Landolt standard stars (Landolt 1992) and spectrophotometric standards (Massey et al. 1988). The FWHM is $\sim 0\farcs7$ on all the composite images, which were obtained under photometric conditions, and for the HDF the narrow band reaches a 1 σ limiting AB magnitude of 26.8 in a 3″ diameter aperture, corrected to a total magnitude following the procedures of Cowie et al. (1994). The corresponding 1 σ flux limit is 6×10^{-18} ergs cm^{-2} s^{-1} over a 3″ diameter aperture. For SSA 22 the 1 σ limit is 0.7 mag fainter, and the flux limit is 3×10^{-18} ergs cm^{-2} s^{-1}.

For the HDF, additional V and I data were obtained with the UH8K camera at the Canada-France-Hawaii Telescope (CFHT; Barger et al. 1998) on the nights of UT 1997 April 3–8. These comprise 22 × 1200 s I-band exposures (8.3 hr) and 33 × 1200 s V-band exposures (11 hr) under conditions of mixed transparency. Net image quality is $\sim 0\farcs8$ FWHM in I and $\sim 0\farcs9$ in V on these exposures. The UH8K V data were registered to the LRIS data, and a noise-weighted addition was performed. The I-band data were calibrated using shallower images obtained under photometric conditions with the University of Hawaii 2.2 m telescope. The corresponding 1 σ limits for the combined HDF observations over a corrected 3″ diameter aperture are 27.2 (B), 27.4 (V), and 25.8 (I), where B and V are on the Johnson system and I is Kron-Cousins. For SSA 22 the corresponding limits are 27.8 (B), 27.5 (V), and 25.8 (I).

Two catalogs were next generated. The first was a narrowband catalog of all objects selected to lie above a surface brightness of 27.9 mag arcsec^{-2} (AB) in a $0\farcs8$ boxcar–smoothed narrowband image, and above a 5 σ limiting aperture magnitude $N(\mathrm{AB}) = 25$ for the HDF and 25.7 for SSA 22. B, V, and I magnitudes were measured for all these objects, and redshifts compiled from the literature (Songaila et al. 1994; Steidel et al. 1996a; Cowie et al. 1996; Cohen et al. 1996; Lowenthal et al. 1997; Steidel et al. 1998) and from unpublished spectroscopy by our group, which may be found in the Hawaii Active Catalog of the HDF.[4] The combined narrowband catalogs contain 1574 objects brighter than $N(\mathrm{AB}) = 25$, of which 412 have spectroscopic identifications, and for SSA 22 an additional 286 objects with $25 < N(\mathrm{AB}) < 25.5$, of which only 10 have spectroscopic identifications. A second V-selected catalog was generated consisting of all objects with surface brightnesses above 29.1 mag arcsec^{-2} in the $0\farcs8$-smoothed V image and with $V < 25.7$ (the 5 σ limit for the HDF). B, V, and N(AB) magnitudes were measured for these objects, and redshifts were compiled. The V-selected catalog contains 2375 objects, of which 457 have spectroscopic identifications. Because the center of the narrowband filter lies very close to the center of the V filter, there is only a very small color difference term. In the subsequent discussion, we use $N = N(\mathrm{AB}) + 0.11 - 0.04(V-I)$ to correct for this. The magnitudes in the SSA 22 field have also been corrected for a small amount of Galactic extinction ($E_{B-V} = 0.05$) using a standard reddening law.

In Figure 1, we show the LRIS fields of the narrowband exposures over a 380″ × 275″ region for the HDF (Fig. 1*a*) and over a 390″ × 280″ region for SSA 22 (Fig. 1*b*). The catalog field corresponds to objects within the central $6\farcm0 \times 4\farcm2$ region, providing similar coverage to other $z > 4$ Lyα narrowband surveys around quasars (e.g., Hu & McMahon 1996) that will be discussed in later papers, or an area roughly 4.4 times the size of the HDF proper. Objects with observed equivalent widths in excess of 77 Å in the narrowband catalog are circled; objects that in addition have measured redshifts within this sample are circled with double borders (here just the $z = 3.430$ object in the HDF found by Lowenthal et al. 1997 and shown in Fig. 1*a*). Image ghosts can be seen around the brightest objects in the fields but do not significantly change the sampling area or sensitivity limits. Figure 2 shows the corresponding regions for the Keck V-band images of the HDF (Fig. 2*a*; redshift identifications are given in Fig. 2*b*) and SSA 22 (Fig. 2*c*). In these images circles indicate the $V < 25.5$ objects that are red in $B-V$ and blue in $V-I$ ($B-V > 1.1$, $V-I < 1.6$). Again, objects circled with double borders in each figure have measured redshifts, in addition to matching the specified color criteria. In the two fields, eight of these objects are $z > 2.9$ galaxies (including one quasar), four are galaxies near $z \sim 0.3$, and two are stars. The HDF is richer in such objects than SSA 22 by a factor of roughly 2.5, suggesting that there is substantial variation in the surface density of $z > 3$ objects from field to field for images with areas of this size.

3. EMISSION-LINE OBJECTS SELECTED BY THE NARROWBAND FILTER

In Figure 3, we plot $V-N$ versus N for the objects in the narrowband-selected catalog. The solid lines show the 3 σ errors. The dashed lines show the $V-N$ color for objects that would have Lyα equivalent widths in excess of 77 Å (that is, in which the flux in the narrow band is double that of the continuum). The vertical bars show the expected $V-N$ range for objects with observed equivalent widths from 77 Å to ∞. The square shows the Lowenthal et al. object. In the HDF there are five objects in the field with observed equivalent widths in excess of 77 Å and with $N < 25$, and in SSA 22 there are seven such objects with $N \leq 25.5$. The fluxes, equivalent widths, V magnitudes, and colors of the objects are summarized in Table 1. The equivalent widths of most of the objects are such that they are unlikely to be [O II] emitters, since the rest-frame [O II] equivalent width rarely exceeds 100 Å (see, e.g., Songaila et al. 1994), and indeed, for the one spectroscopically identified object the emission is caused by Lyα, which is the only plausible alternate. We therefore consider these objects as the candidate sample of strong Lyα emitters and attempt to confirm this with other diagnostics.

In Figure 4, we plot the locus of the $V-I$ versus $B-V$ colors for the narrowband-selected objects in the LRIS fields and compare these with the color distribution of V-selected catalog objects in the HDF proper, and V-selected objects in the LRIS image of the SSA 22 field. The objects

[4] http://www.ifa.hawaii.edu/~cowie/tts/tts.html.

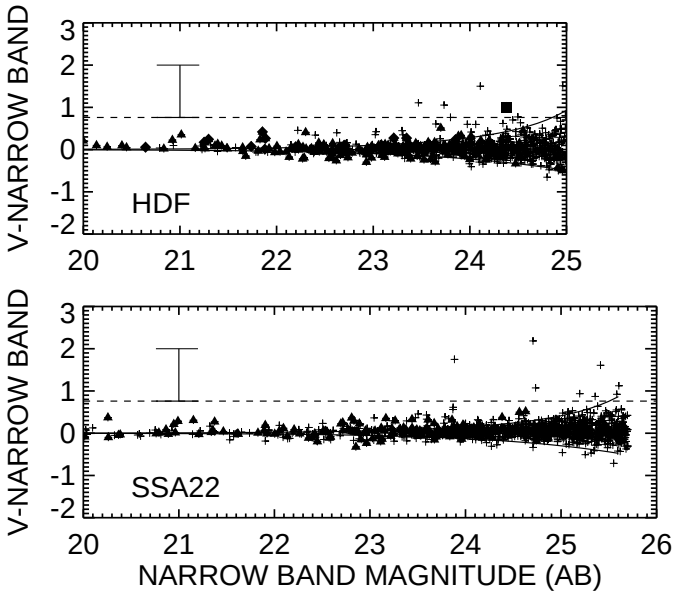

FIG. 3.—Distribution of emission-line excess $V-N$ vs. N for objects (*plus signs*) in the narrowband catalogs for the HDF and SSA 22. The solid lines show the distribution of 3 σ errors. The square shows the Lowenthal et al. $z = 3.430$ object, the diamonds objects for which [O II] λ3727 falls in the filter bandpass, and the triangles other objects with measured redshifts. The dashed lines show the $V-N$ color corresponding to an equivalent width of 77 Å, and the vertical bars show the expected $V-N$ distribution for objects with observed equivalent widths ranging from 77 Å to ∞.

(*filled squares*) that meet our equivalent width criterion and that are bright enough in the continuum for colors to be measured (Table 1) have predominantly red $B-V$ colors but are blue (or close to flat-spectrum f_ν) in $V-I$ colors, as would be expected for high-redshift objects that are dominated by star formation (Cowie 1988; Songaila, Cowie, & Lilly 1990; Steidel et al. 1996a, 1996b; Lowenthal et al. 1997). These objects occupy the same region of the color-color diagram as objects seen in the tail of the color-color distribution for the HDF proper at blue $V-I$ (or F602W − F814W) and red $B-V$ (Fig. 4, *top right*), and which correspond to high-redshift galaxies selected by color. As we shall demonstrate using the colors of HDF objects with known redshifts, these continuum colors can also distinguish redshift $z \sim 3.4$ objects from lower z emitters. (We also note that the narrowband catalog has a shallower slope in the Fig. 4 color-color diagrams for the HDF, because the F602W filter is redder than the V band used with LRIS.) The color selection criterion is therefore consistent with the interpretation that nearly all of the sample are Lyα emitters.

The redshift information also allows us to check the equivalent width selection procedure. In Figure 5, we show $V-N$ versus redshift, with the redshift intervals matching the narrowband filter bandpass indicated for emission from [O III] λ5007 (at $z \sim 0.08$), [O II] λ3727 (at $z \sim 0.45$), Mg II λ2800 (at $z \sim 0.93$), and Lyα λ1216 (at $z \sim 3.43$). These are the most prominant spectral features in most galaxies (see Songaila et al. 1994; Cowie, Hu, & Songaila 1995), with Mg II normally seen in absorption, and they are clearly seen in the color-redshift plot. The increasing width of the redshift interval corresponding to the narrowband wavelengths at high redshifts is also seen. The scatter of points gives an idea of the real distribution of the signal strength of each feature, and it may also be seen that the high-z Lyα emitter, corresponding to the Lowenthal et al. object, does indeed have an appreciably higher equivalent width than any of the [O II] emitters. We also note that other structures arise from additional spectral features (e.g., the 4000 Å break and Fe II absorption lines) that add to the dispersion.

The color trends shown in Figure 4 can also be examined in more detail by supplementing the measured colors for these objects with redshift information. In Figure 6, we plot $B-V$ colors versus redshift for all galaxies in our V-selected catalog for which this information is available. It may be seen that applying a blue $V-I$ color criterion ($V-I < 1.6$) selects galaxies over a range of redshifts, extending at least to $z \sim 3.5$, but that within this subsample there are very definite trends in $B-V$ color with redshift. This function ($B-V$ vs. redshift) remains double-valued out to about $z \sim 3$, with a progressive decrease (blueing) in $B-V$ color as the 4000 Å Balmer break moves out of the B band to longer wavelengths in the observed frame. At higher redshifts, the combination of the Lyman break and the depression of the continuum below Lyα as a result of increasing

TABLE 1

PROPERTIES OF STRONG EMITTERS

ID	Flux (10^{-17} ergs cm^{-2} s^{-1})	W_λ (observed) (Å)	V	$V-I$	$B-V$	z
HDF, $N < 25$:						
LA 1.....	8.0	140	24.6	0.9	1.1	...
LA 2.....	6.1	135	24.8	0.5	1.4	...
LA 3.....	5.2	250	25.7	0.0	2.2	...
LA 4.....	3.2	115	25.4	1.6	1.9	3.430[a]
LA 5.....	2.4	250	26.5	0.2	1.1	...
SSA 22, $N < 25.5$:						
LA 1.....	6.7	325	25.7	0.8	2.4	3.455[b]
LA 2.....	5.2	230	25.6	0.8	1.6	3.460[b]
LA 3.....	3.8	>845	−28.0[c]	...	...	3.450[b]
LA 4.....	2.5	140	25.9	0.2	1.3	...
LA 5.....	2.0	>405	−28.7[c]	...	...	...
LA 6.....	1.5	115	26.2	0.4	1.0	...
LA 7.....	1.2	90	26.2	2.2	1.2	...

[a] Lowenthal et al. 1997.

[b] Hu et al. 1998.

[c] A negative V magnitude here indicates that there is a negative flux in the aperture. The 1 σ limits on V are 27.4 (HDF) and 27.5 (SSA 22).

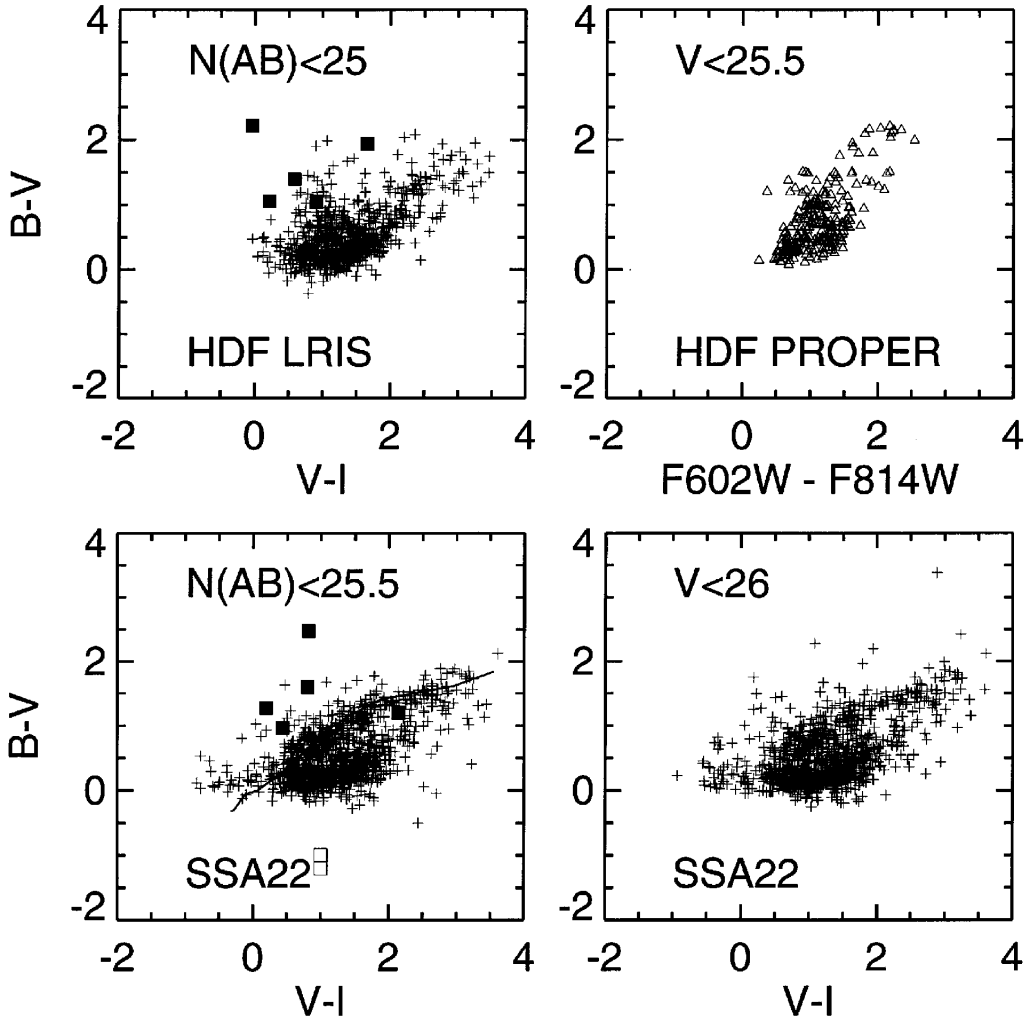

FIG. 4.—$B-V$ vs. $V-I$ color-color plots for objects in the HDF and SSA 22 fields selected from the narrowband and V-band catalogs. The left panels show the color distributions of objects in the narrowband catalogs [N(AB) < 25 for the LRIS HDF field and N(AB) < 25.5 for the LRIS SSA 22 field]. The colors of emission-line objects in these magnitude-selected catalogs with equivalent widths in excess of 77 Å in the observed frame are indicated by filled squares, and may be seen to lie at red $B-V$ and blue $V-I$ colors. Two of the strong emission-line objects in the SSA 22 field have continuua that are either undetected or too faint to provide color measurements (Table 1). They are indicated schematically by open squares placed at nominal color positions. The slightly higher density of stars in the SSA 22 field ($b \sim -44°$) compared with the HDF ($b \sim +55°$) may be seen in the more populated star track (*solid line*) that approaches the blue end of the high-z galaxy color distribution. The right panels show the color distribution of objects from our V-selected catalogs ($V < 25.5$ for the HDF and $V < 26$ for SSA 22). For the HDF, the available *HST* filter measurements provide a tighter color distribution, and here we have elected to use F602W − F814W in place of $V-I$ and F450W − F602W in place of $B-V$, with the $V < 25.5$ sample restricted to the HDF proper (about a quarter of the size of the larger LRIS field). These points are shown as triangles. The steeper slope of this color distribution is a reflection of the different wavelength center (i.e., F602W vs. V) used for the horizontal axis.

absorption by Lyα forest clouds leads to progressively redder observed $B-V$ colors, and $z > 3$ galaxies are easily distinguished. The data show that using the color criteria $V-I < 1.6$ and $B-V > 1.1$ will select primarily $z \gg 3$ galaxies, though with a small admixture of low-redshift galaxies and stars.

In Figure 7, we show how local continuum shape can be used to discriminate between the three classes of emission line ([O II], [O III], and Lyα) that produce significant equivalent widths in the narrow band and, hence, to identify weaker Lyα emitters than would be picked out by the strong equivalent width criterion used previously. For the low-redshift [O III] lines, the continuum is flat and $B-V < 0.4$ (*bottom*). For the [O II] lines there is a strong discontinuity just redward of 3727 Å (see, e.g., Lilly et al. 1995), which places $B-V$ in the 0.4–1.0 range. Finally, for the Lyα lines the strong discontinuity produced by the Lyα forest across the Lyα line places $B-V$ above 1.0 (Cowie 1988; Madau et al. 1996).

We have divided the entire sample [N(AB) < 25 in the HDF, N(AB) < 25.5 in SSA 22] in the same way in Figure 8. Here it can be seen that the $B-V$ sample selects out the highest equivalent width objects, with only one object falling into the $B-V < 1$ class, having $V-N > 0.78$. As is illustrated in the top panel of Figure 8, the $V-N > 0.5$, $B-V > 1$ criterion should be effective in picking out emitters. However, weaker $V-N$ cuts become contaminated by error and color spread. The color-enhanced selection criterion therefore yields only a small number of additional objects over the simple strong equivalent width criterion.

4. DISCUSSION

The strong equivalent width criterion yields 10 strong Lyα emitters with flux above 2×10^{-17} ergs cm^{-2} s^{-1} in

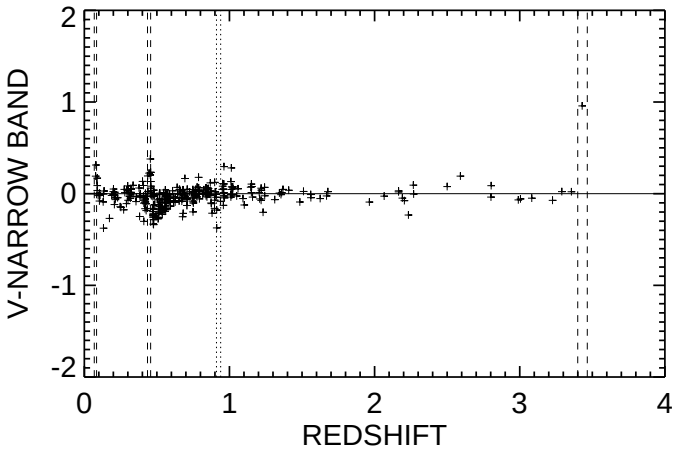

FIG. 5.—Excess emission in narrow band over V band vs. redshift for objects in the HDF and SSA 22 fields. Objects with spectroscopic identifications in the literature (Lowenthal et al. 1997; Cohen et al. 1996; HDF Active Catalog Web page; Steidel et al. 1996a) over the HDF and SSA 22 fields sampled by the LRIS deep-imaging fields are shown here. The positions and redshift ranges corresponding to features such as Mg II (*dotted lines*) and [O III], [O II], and Lyα (*dashed lines*) falling within the filter bandpass are indicated. The structure of the continuum near the [O II] feature can be seen reflected in both the "dip" and dispersion of points in this region, and it can also be seen that emission-line objects in [O II] and a few [O III] emitters may be detected. Underlying continuum features can also increase the dispersion of these points in different redshift regions. At higher redshifts a correspondingly wider redshift region is sampled by the filter bandpass. Redshifts used only include values known at the time of the imaging observations, and do not include follow-up spectroscopic confirmations of candidate Lyα emitters, which will be described in Hu et al. (1998).

the 46 arcmin^2 field coverage (about 800 deg^{-2}) lying in the redshift range $z = 3.405$–3.470, or roughly 13,000 per unit z per square degree. Two of these objects—both lying in the SSA 22 region—are completely undetected in the continuum at the 1 σ level of $V = 27.5$, while the remainder have V magnitudes ranging from 24.6 to 26.5 (Table 1). To a $V = 25.5$ mag limit, a color criterion $B-V > 1.1$, $V-I < 1.6$ of the type discussed above yields 72 objects within the sample area when known low-redshift galaxies or stars are excluded. If we assume a rough z range of 3.1–3.5,

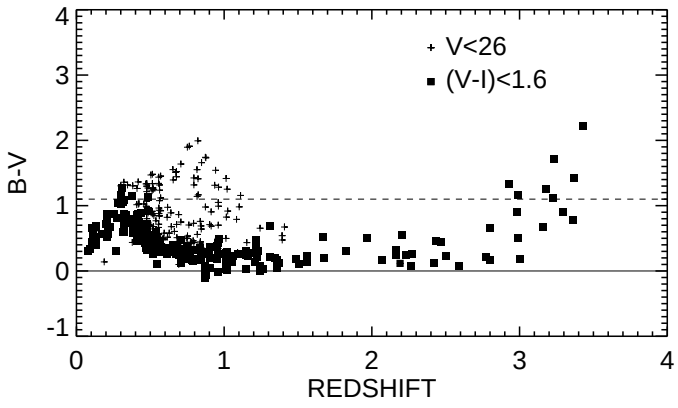

FIG. 6.—$B-V$ vs. redshift for SSA 22 and the HDF. For objects with known redshifts in these two fields, the $V < 26$ sample (*plus signs*) is divided according to $V-I$ color. For those objects that are relatively blue in $V-I$ colors ($V-I < 1.6$) (*squares*), a clear trend in $B-V$ color with redshift may be seen, corresponding to passage of continuum break features through the reference bandpasses. At high redshifts ($z \gtrsim 2.9$) star-forming galaxies, which will have flat $V-I$ spectra, appear extremely red in $B-V$, and may be selected by their color breaks. A dashed reference line at $B-V$ corresponds to our $B-V$ color selection.

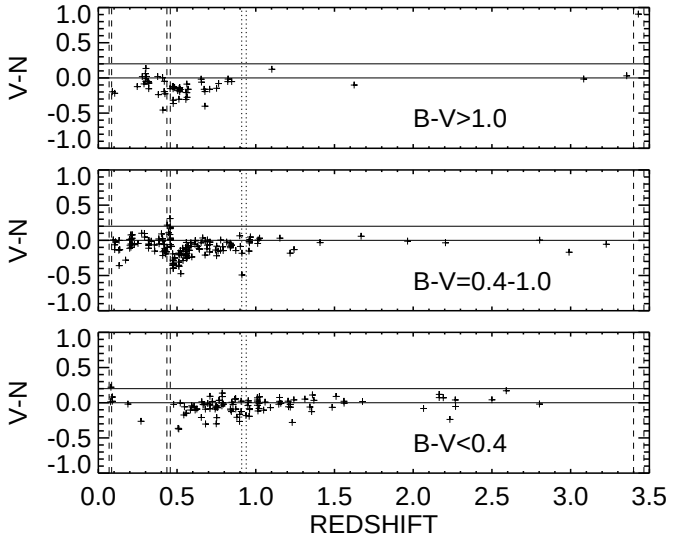

FIG. 7.—$V-N$ vs. redshift for objects with $N(\mathrm{AB}) < 24.5$ in three $B-V$ color subsamples. The data are grouped according to $B-V$ color and illustrate the color trends with redshift of Fig. 6, which demonstrates that it is possible to discriminate between classes of emitters using color data, and hence to identify weaker Lyα emitters than would be possible with a strong equivalent width criterion. The solid lines show objects with $V-N > 0.2$. For $B-V > 1.0$ the identified emission-line object corresponds to Lyα at $z \sim 3.4$. In the intermediate $0.4 < B-V < 1.0$ color range, [O II] emission-line objects are selected. At $B-V < 0.4$ the narrowband excess objects correspond to [O III] emitters.

where the upper limits are determined by the passage of the Lyα forest through the middle of the V band, this selection also corresponds to a surface density of 13,000 per unit z per square degree. While the number is quite uncertain because of the small number statistics, the choice of magnitude limit, and the possibility of redshift clustering, there are comparable numbers of strong Lyα emitters and color-selected galaxies at these flux selection limits. This is consistent with the spectroscopic properties of the color-selected objects with measured high redshifts, and it appears that Lyα emission is quite common in the high-redshift objects. In addition, there appear to be numbers of bare Lyα emitters where the

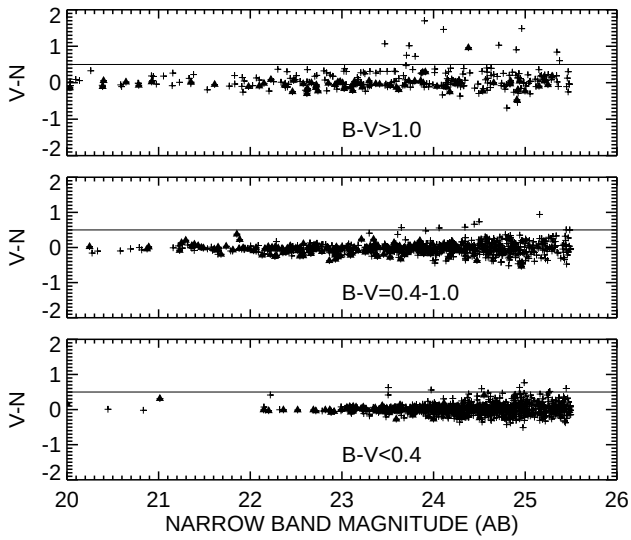

FIG. 8.—$V-N$ vs. N for $N(\mathrm{AB}) < 25$ in the HDF and $N(\mathrm{AB}) < 25.5$ in SSA 22 divided by $B-V$ color into three bins. Objects with known redshifts are marked with triangles. The dividing line in $V-N$ is set at 0.5.

continuum is undetectable, which balances to some extent the presence of color-selected objects without strong emission.

In the absence of extinction and with the assumption that the Lyα emission is produced by photoionization by stars, the conversion from Lyα luminosity to star formation rate (SFR) is 1 $M_\odot$ yr^{-1} = 10^{42} ergs s^{-1} in the Lyα line, where we have used Kennicutt's (1983) relation between the star formation rate and Hα luminosity and the case B Lyα/Hα = 8.7 (Brocklehurst 1971). Because of the effects of extinction, the Lyα luminosity is likely to underestimate the SFR, while if some portion of the Lyα luminosity is powered by AGNs we will overestimate the SFR. The size of these effects is not easy to estimate, though the rest-frame equivalent widths of the lines (Table 1) imply that if the objects are photoionized, then extinction cannot reduce the line luminosities by more than a factor of about 2 before reasonable theoretical upper bounds on the equivalent width (Charlot & Fall 1993) are exceeded. We also note that in the spectra obtained to date of the SSA 22 emitters (Hu, Cowie, & McMahon 1998) there is little sign of the C IV line that might indicate AGN activity.

Proceeding therefore under the assumption that the line is photoionized by stars and neglecting extinction, we find maximum star formation rates of just under 10 h_{50}^{-2} $M_\odot$ yr^{-1} for $q_0 = 0.5$, which are very similar to those seen at lower z (Cowie et al. 1997) and those inferred from the continuum light of color-selected objects at these redshifts (Steidel et al. 1998). In Figure 9, we show the Lyα luminosity function constructed for $H_0 = 65$ km s^{-1} Mpc^{-1} and $q_0 = 0.5$. In the absence of extinction, this may be directly converted to an $\dot{M}$ distribution using the L(Lyα)-$\dot{M}$ relation. The $\dot{M}$ function is quite similar to that seen at $z = 1$ (Cowie et al. 1997) within the large statistical uncertainties and modulo the different methodologies used (UV fluxes vs. Lyα luminosities). It is more probable that $\dot{M}$ is underestimated at the high redshift, because extinction must have a larger effect on the Lyα line than on the continuum. Integrating through the $\dot{M}$ function, we find a star formation density of

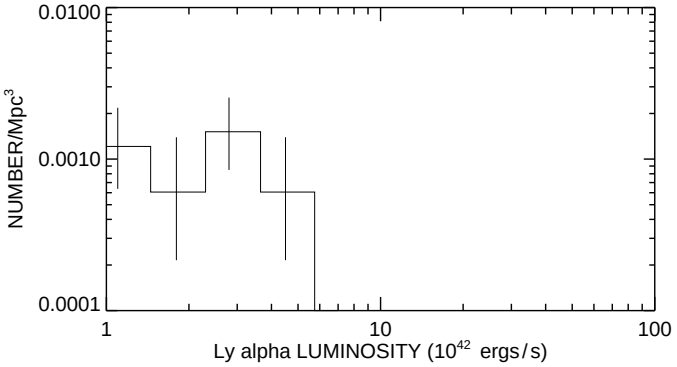

FIG. 9.—Distribution of Lyα emission vs. Lyα luminosity for the strong equivalent width emission-line objects in the SSA 22 and HDF LRIS fields. The horizontal axis may be converted to star formation rate in the absence of extinction and assuming that the Lyα is produced by photoionization, whence 10^{42} ergs s^{-1} ≈ 1 $M_\odot$ yr^{-1}. The errors are ± 1 σ, based on the number of objects in each bin. See text for a more extensive discussion.

0.01 $M_\odot$ Mpc^{-3} yr^{-1}, which is quite similar to that inferred from color arguments (e.g., Madau et al. 1996; Mobasher & Mazzei 1997). Again, it must be emphasized that this is an extreme lower limit, since we neglect extinction.

We thank Boris Shnapir for assistance in the design and fabrication of the narrowband filter, Bob Williams and Richard Ellis for comments on an earlier draft of this paper, and Tom Bida and Bob Goodrich for their assistance in obtaining the observations, which would not have been possible without the LRIS spectrograph of Judy Cohen and Bev Oke. Support for this work was provided by the state of Hawaii and by NASA through grants GO-5975.01-94A, GO-06222.01-95A, and AR-06377.06-94A from the Space Telescope Science Institute, which is operated by AURA, Inc., under NASA contract NAS 5-26555. E. M. H. would also like to gratefully acknowledge a University Research Council Seed Money Grant.

REFERENCES

Barger, A., et al. 1998, AJ, submitted
Brocklehurst, M. 1971, MNRAS, 153, 471
Charlot, S., & Fall, S. M. 1993, ApJ, 415, 580
Cohen, J. G., Cowie, L. L., Hogg, D. W., Songaila, A., Blandford, R., Hu, E. M., & Shopbell, P. 1996, ApJ, 471, L5
Cowie, L. L. 1988, in The Post-Recombination Universe, ed. N. Kaiser & A. N. Lasenby (NATO ASI Ser. C, 240) (Dordrecht: Kluwer), 1
Cowie, L. L., Gardner, J. P., Hu, E. M., Songaila, A., Hodapp, K. W., & Wainscoat, R. J. 1994, ApJ, 434, 114
Cowie, L. L., Hu, E. M., & Songaila, A. 1995, Nature, 377, 603
Cowie, L. L., Hu, E. M., Songaila, A., & Egami, E. 1997, ApJ, 481, L9
Cowie, L. L., Songaila, A., Hu, E. M., & Cohen, J. G. 1996, AJ, 112, 839
Djorgovski, S. G., Pahre, M. A., Bechtold, J., & Elston, R. 1996, Nature, 382, 234
Djorgovski, S., Spinrad, H., McCarthy, P., & Strauss, M. 1985, ApJ, 299, L1
Francis, P. J., Woodgate, B. E., & Danks, A. C. 1997, ApJ, 482, L25
Francis, P. J., et al. 1996, ApJ, 457, 490
Hu, E. M., Cowie, L. L., & McMahon, R. G. 1998, ApJL, submitted
Hu, E. M., & McMahon, R. G. 1996, Nature, 382, 231
Hu, E. M., McMahon, R. G., & Egami, E. 1996, ApJ, 459, L53
———. 1997, in The Hubble Space Telescope and the High Redshift Universe, ed. N. Tanvir, A. Aragón-Salamanca, & J. Wall (Singapore: World Sci.), 91
Kennicutt, R. C., Jr. 1983, ApJ, 272, 54
———. 1992, ApJ, 388, 310
Landolt, A. U. 1992, AJ, 104, 340
Lilly, S. J., Le Fèvre, O., Crampton, D., Hammer, F., & Tresse, L. 1995, ApJ, 460, L1
Lowenthal, J. D., et al. 1997, ApJ, 481, 673
Macchetto, F., Lipari, S., Giavalisco, M., Turnshek, D. A., & Sparks, W. B. 1993, ApJ, 404, 511
Madau, P., Ferguson, H. C., Dickinson, M. E., Giavalisco, M., Steidel, C. C., & Fruchter, A. 1996, MNRAS, 283, 1388
Massey, P., Strobel, K., Barnes, J. V., & Anderson, E. 1988, ApJ, 328, 315
Mobasher, B., & Mazzei, P. 1997, MNRAS, submitted
Oke, J. B., et al. 1995, PASP, 107, 375
Pascarelle, S. M., Windhorst, R. A., Keel, W. C., & Odewahn, S. C. 1996, Nature, 383, 45
Petitjean, P., Pécontal, E., Valls-Gabaud, D., & Charlot, S. 1996, Nature, 380, 411
Pritchet, C. J. 1994, PASP, 106, 1052
Songaila, A., Cowie, L. L., Hu, E. M., & Gardner, J. P. 1994, ApJS, 94, 461
Songaila, A., Cowie, L. L., & Lilly, S. J. 1990, ApJ, 348, 371
Steidel, C. C., Adelberger, K., Dickinson, M., Giavalisco, M., Pettini, M., & Kellogg, M. 1998, ApJ, 492, 428
Steidel, C. C., Giavalisco, M., Dickinson, M., & Adelberger, K. L. 1996a, AJ, 112, 352
Steidel, C. C., Giavalisco, M., Pettini, M., Dickinson, M., & Adelberger, K. L. 1996b, ApJ, 462, L17
Williams, R. E., et al. 1996, AJ, 112, 1335